The Atmospheric Oxidation of Ethyl Formate and Ethyl Acetate over a Range of Temperatures and Oxygen Partial Pressures

John J. Orlando and Geoffrey S. Tyndall,
Atmospheric Chemistry Division, Earth and Sun Systems Laboratory,
National Center for Atmospheric Research, Boulder CO 80305

Revised version submitted to International Journal of Chemical Kinetics, January 2010.

Abstract

The Cl-atom initiated oxidation of two esters, ethyl formate [$HC(O)OCH_2CH_3$] and ethyl acetate [$CH_3C(O)OCH_2CH_3$], has been studied near 1 atm. as a function of temperature (249 – 325 K) and O_2 partial pressure (50-700 Torr) using an environmental chamber technique. In both cases, Cl-atom attack at the CH_2 group is most important, leading in part to the formation of radicals of the type $RC(O)OCH(O\bullet)CH_3$ [R=H, CH_3]. The atmospheric fate of these radicals involves competition between reaction with O_2 to produce an anhydride compound, $RC(O)OC(O)CH_3$, and the so-called α-ester rearrangement which produces an organic acid, RC(O)OH and an acetyl radical, $CH_3C(O)$. For both species studied, the α-ester rearrangement is found to dominate in 1 atm. air at 298 K. Barriers to the rearrangement of 7.7±1.5 and 8.4±1.5 kcal/mole are estimated for $CH_3C(O)OCH(O\bullet)CH_3$ and $HC(O)OCH(O\bullet)CH_3$, respectively, leading to increased occurrence of the O_2 reaction at reduced temperature. The data are combined with those from similar studies of other simple esters to provide a correlation between the rate of occurrence of the α-ester rearrangement and the structure of the reacting radical.

Introduction

Esters are emitted into the atmosphere from natural (e.g., biomass burning and vegetation) and anthropogenic (e.g., from use as industrial solvents and in perfumes and flavorings manufacturing) sources, and are also formed *in situ* from the oxidation of ethers [e.g., references 1-25 and refs. therein]. Thus, the atmospheric oxidation of these species has the potential to contribute to air quality on regional and global scales. Although the esters are reasonably unreactive (lifetimes against reaction with OH range from a few days to a couple of months for C_3-C_5 formates and acetates, [e.g., refs. 2-4,8,10,19,26,27]) and are not likely major sources of ozone in urban regions [28], their

main oxidation products are often soluble organic acids and acid anhydrides [5-15,25,29] which may contribute to the atmospheric buildup of condensed-phase organic mass.

As with most volatile organic compounds, atmospheric oxidation will be initiated mainly by reaction with OH, and will lead to the production of a peroxy, and subsequently an alkoxy radical, as shown below for a generic ester, $RC(O)OCH_2R'$ [30]:

$$OH + RC(=O)OCH_2R' (+ O_2) \rightarrow \quad RC(=O)OCH(OO\bullet)R' + H_2O$$

$$RC(=O)OCH(OO\bullet)R' + NO \rightarrow \quad RC(=O)OCH(O\bullet)R' + NO_2$$

A key step in the oxidation of the esters, and the major source of the organic acids, is the so-called α-ester rearrangement [5] of the alkoxy radical, which can occur in competition with reaction of the alkoxy species with O_2, e.g., :

$$RC(=O)OCH(O\bullet)R' \rightarrow \quad RC(=O)OH + R'C\bullet O$$

$$RC(=O)OCH(O\bullet)R' + O_2 \rightarrow \quad RC(=O)OC(=O)R' + HO_2$$

The α-ester rearrangement process was first discovered by Tuazon et al. [5] in their study of the atmospheric oxidation of ethyl, isopropyl, and t-butyl acetate, and its occurrence has subsequently been confirmed in theoretical [13,14] and experimental [7-12,15,25] studies of these and other esters, including methyl and ethyl formate, methyl acetate, methyl propionate, methyl pivalate, n-propyl acetate and isobutyl acetate. Although it is now apparent that the α-ester rearrangement occurs more rapidly for larger and more-substituted alkoxy radicals, there is still limited information available regarding the energetics and dynamics of this process for the suite of atmospherically relevant esters.

In this paper, we describe an environmental chamber study of the oxidation of ethyl formate and ethyl acetate, the major products of the atmospheric oxidation of diethyl ether [16,18,20,31]. These studies were carried out over a range of temperatures (249-325 K) and O_2 partial pressures (50-700 Torr) to examine competition, under conditions relevant to the lower atmosphere, between the α-ester rearrangement and reaction with O_2 for the $HC(O)OCH(O\bullet)CH_3$ and $CH_3C(O)OCH(O\bullet)CH_3$ radicals derived from ethyl formate and ethyl acetate. The data allow activation barriers to the α-ester rearrangement to be determined, and these values are compared to previous estimates [13-15] for related species.

Experimental

Experiments were carried out using a 2 m long, 47 L stainless steel environmental chamber system, that has been described previously [15,31,32]. The chamber temperature was controlled using either chilled ethanol (T < 298 K) or heated water (T > 298 K) that was flowed through a jacket surrounding the cell from temperature-regulated circulating baths. Analysis of the gas mixtures in the chamber was conducted using Fourier transform infrared (FTIR) spectroscopy. Multi-pass optics (modified Hanst-type) housed within the chamber provided an infrared observational path of 32 m. Infrared spectra were recorded over the range 800-3900 cm^{-1}, and were obtained at a resolution of 1 cm^{-1} from the co-addition of 200 scans (acquisition time 3-4 minutes).

Experiments involved the irradiation of mixtures of Cl_2 (14-51 x 10^{15} molecule cm^{-3}) and the parent ester (0.9-2.5 x 10^{14} molecule cm^{-3}) in O_2 (50-700 Torr) / N_2 (balance) buffer gas at total pressures of 720-770 Torr, and at temperatures ranging from 249 to 325 K. Minor components of the gas mixtures were flushed into the chamber from smaller calibrated volumes using a flow of N_2, while the O_2 was added directly to the chamber. A Xe-arc lamp, filtered to provide radiation in the 240-400 nm range, was used to photolyze Cl_2 and thus initiate the chemistry. Typically, mixtures were photolyzed for 4-6 periods, each of duration 15-200 s, and an infrared spectrum was recorded after each photolysis period. In limited cases, to minimize heterogeneous loss of reaction products, gas mixtures were photolyzed continuously and IR spectra were recorded sequentially throughout the photolysis period.

Quantification of the parent esters (ethyl formate or ethyl acetate) and most major products [formic acid (FA), CO, CO_2, acetic acid, and acetic acid anhydride (AAn)] was carried out using standard spectra recorded on our system at the temperature at which the experiments were conducted. Quantification of formic acid anhydride (FAn) and acetic formic anhydride (AFAn), both products of ethyl formate oxidation, was via integrated band intensities obtained from room temperature reference spectrum provided by Tim Wallington, Ford Motor Company. Some minor products (e.g., CH_3OH, CH_2O, peracetic acid and acetic acid) were quantified via comparison with reference spectra obtained at 298 K.

A series of control experiments revealed that the two esters under investigation were not subject to significant heterogeneous loss in the chamber, and were not photolyzed over the time period of experiments conducted herein. While heterogeneous losses of most major products were minor, it was observed that formic acid, a major product of ethyl formate oxidation, was prone to significant heterogeneous loss. To minimize this loss, many experiments were conducted using the "continuous photolysis" method described above. In most cases, corrections (usually < 10%) were made to account for this loss. However, results from some early experiments, in which no corrections were made, were indistinguishable from later experiments and were used in the analysis. Quantitative analyses to be presented in this paper are based primarily on yields of formic acid (FA) and AFAn (from ethyl formate) or acetic acid and AAn (from ethyl acetate). These product species are known (or estimated) to react approximately 100 times slower with Cl-atoms than do the parent esters [7,22-24,29,33-36]; hence, no correction for secondary loss of these product species was required.

Chemicals used in this study were from the following sources: Cl_2 (Matheson, UHP); ethyl formate (97%), ethyl acetate (99.5+%), acetic acid (99.8%), formic acid (95%), acetic acid anhydride (98%+), all Sigma-Aldrich; O_2 (U.S. Welding); N_2, (boil-off from liquid N_2, U.S. Welding). Gases (Cl_2, N_2, O_2) were used as received, liquids (ethyl formate, ethyl acetate, acetic acid, formic acid, acetic acid anhydride) were subjected to several freeze-pump-thaw cycles before use.

Results and Discussion

1) Ethyl Formate at 298 K

Products identified in the Cl-atom initiated oxidation of ethyl formate at 298 K included CO_2, CO, FA, AFAn, peracetic acid, formic acid anhydride (FAn), and in some cases trace amounts of formaldehyde and possibly trace amounts of acetic acid and methanol. On average, these products accounted for about 86±15% of the reacted ethyl formate on a carbon basis. Results from typical experiments carried out at 298 K in 1 atm air, plotted as observed product concentrations versus ethyl formate consumption (appearance profiles), are displayed in Figure 1. The appearance profiles for CO_2, CO, formic acid, AFAn, and peracetic acid appear linear within experimental uncertainty,

indicating that these may be primary products. However, consideration of the chemistry involved shows that some of the CO and CO_2 results from rapid consumption of reactive first-generation products, such as formaldehyde and acetaldehyde. After removal of spectral features due to known products, residual absorption features remained in the product spectra at 1115, 1166, 1345, 1455, and 1773 cm^{-1}. Likely contributors to the unidentified absorption features (and to the missing carbon) include hydroperoxides, carbonyls and alcohols that can be obtained from molecular channels of peroxy radical reactions, as discussed in more detail below.

Yields of most products were found to be dependent on O_2 partial pressure (see Table 1). Yields of FA, CO_2 and CO decreased with increasing O_2, while those of AFAn and FAn increased. As is quantitatively discussed below, the majority of these effects stem from the $HC(O)OCH(O\bullet)CH_3$ species, whose chemistry involves competition between O_2 reaction to form AFAn and α-ester rearrangement to, in essence, form FA, CO and CO_2.

To quantitatively determine the origin of the identified products, and to examine the origin of the O_2 dependence of their yields, the branching ratios to the three possible sites of Cl-atom attack on ethyl formate must first be determined:

$$Cl + HC(O)OCH_2CH_3 \rightarrow \bullet C(O)OCH_2CH_3 + HCl \quad (1a)$$

$$Cl + HC(O)OCH_2CH_3 \rightarrow HC(O)OCH\bullet CH_3 + HCl \quad (1b)$$

$$Cl + HC(O)OCH_2CH_3 \rightarrow HC(O)OCH_2CH_2\bullet + HCl \quad (1c)$$

To determine the branching ratio to reaction at the formate group, reaction (1a), experiments were conducted with NO_2 (3.5-7 x 10^{14} molecule cm^{-3}) added to standard Cl_2/ethyl formate/air mixtures. Under these conditions, the radical product of reaction (1a) is converted quantitatively to a stable PAN-type compound [9,25], designated here as ethoxyPAN or EoPAN:

$$Cl + HC(O)OCH_2CH_3 \rightarrow \bullet C(O)OCH_2CH_3 + HCl \quad (1a)$$

$$\bullet C(O)OCH_2CH_3 + O_2 \rightarrow \bullet O_2C(O)OCH_2CH_3 \quad (2a)$$

$$\bullet O_2C(O)OCH_2CH_3 + NO_2 \rightarrow O_2NO_2C(O)OCH_2CH_3 \text{ (EoPAN)} \quad (3a)$$

Formation of the EoPAN will be accompanied by the production of less thermally stable alkyl peroxynitrates, as shown below for channel (1b):

$$Cl + HC(O)OCH_2CH_3 \rightarrow HC(O)OCH\bullet CH_3 + HCl \quad (1b)$$

$HC(O)OCH\bullet CH_3 + O_2 \rightarrow HC(O)OCH(OO\bullet)CH_3$ (2b)

$HC(O)OCH(OO\bullet)CH_3 + NO_2 \leftrightarrow HC(O)OCH(OONO_2)CH_3$ (3b)

To allow separation of the spectral contributions of EoPAN and the alkyl peroxynitrates, excess NO (7-55 x 10^{14} molecule cm^{-3}) was added to the photolyzed mixtures to remove the alkylperoxynitrate species, e.g.,

$HC(O)OCH(OONO_2)CH_3 \rightarrow HC(O)OCH(OO\bullet)CH_3 + NO_2$ (-3b)

$HC(O)OCH(OO\bullet)CH_3 + NO \rightarrow HC(O)OCH(O\bullet)CH_3 + NO_2$ (4b)

$HC(O)OCH(O\bullet)CH_3 \rightarrow$ Products

After proper accounting for products generated following NO addition (FA, AFAn and PAN, see below), as well as inorganic species such as $ClNO_2$ and ClNO, spectral features centered at 1166, 1224, 1300, 1745, and 1835 cm^{-1} could be assigned to EoPAN while major alkyl peroxynitrate features were found at 1100, 1160, 1300, 1727 and 1762 cm^{-1}. These features correspond very closely to those attributed [9,37] to the analogous species generated from methyl formate oxidation in the presence of NO_2, $O_2NO_2C(O)OCH_3$ and $HC(O)OCH_2OONO_2$. The EoPAN band positions and relative intensities also agree quite well with those reported by Malanca et al. [25] in a recent study of ethyl formate oxidation, the one exception being the 1166 cm^{-1} band which is absent in the Malanca et al. [25] spectrum. Given this fact, it is likely that the 1166 cm^{-1} band is then due not to EoPAN, but to the presence in our spectra of other multi-functional nitrates or nitrites derived from oxidation of the ethyl group. Note also that, as shown below, most of the Cl-atom reaction occurs at the $-CH_2-$ group in ethyl formate and thus the major contributor to the alkylperoxynitrate absorption spectrum is expected to be the $HC(O)OCH(OONO_2)CH_3$ species.

Determination of the branching ratio to pathway (1a) then requires quantification of the EoPAN formed versus loss of the parent ethyl formate. Spectra of the PAN species formed from methyl, isopropyl and t-butyl formate oxidation in the presence of NO_2 are available from work in our laboratory [9,38], and all show integrated band strengths (for the band centered near 1830 cm^{-1}) of (3.9±0.8) x 10^{-17} cm $molecule^{-1}$ and peak cross sections for this band of (1.9±0.4) x 10^{-18} cm^2 $molecule^{-1}$ Use of these values for EoPAN quantification allows us to conclude that 18±5% of the reaction of Cl-atoms with ethyl formate occurs via pathway (1a). Equivalently, given $k_1 \approx 1.0 \times 10^{-11}$ cm^3

molecule^{-1} s^{-1} [22-24,29,33], then $k_{1a} = (1.8\pm0.5) \times 10^{-12}$ cm^3 molecule^{-1} s^{-1}. This result, however, appears to disagree with the yield of EoPAN (and hence the branching to abstraction of the formyl H-atom) reported by Malanca et al. [25], (44±5%) branching ratio reported in their study compared with our (18±5%) value. However, comparisons of the cross sections used in our work with those of Malanca et al. (provided by the authors of that study via private communication) reveals that their values are roughly a factor of four lower than our estimates. While determination of the exact branching to pathway (1a) awaits clarification of this cross section issue, we do note that use of the Malanca et al. [25] cross sections in the analysis of our data would lead to a sum of the abstraction pathways well in excess of unity.

To conclude our discussion of pathway (1a), it remains to consider the end-products of this pathway in the absence of NO_x. By analogy to the case of methyl formate, addition of O_2 should be the sole fate of the $\bullet C(O)OCH_2CH_3$ radical. Subsequent reaction of the resultant acylperoxy radical with other peroxy radicals present in the system is expected to generate CO_2 and CH_3CHO as first-generation end-products:

$$\bullet C(O)OCH_2CH_3 + O_2 \rightarrow \bullet O_2C(O)OCH_2CH_3 \quad (2a)$$

$$\bullet O_2C(O)OCH_2CH_3 + RO_2 \rightarrow \bullet OC(O)OCH_2CH_3 + RO\bullet + O_2 \quad (5a)$$

$$\bullet OC(O)OCH_2CH_3 \rightarrow CO_2 + \bullet OCH_2CH_3 \quad (6)$$

$$\bullet OCH_2CH_3 + O_2 \rightarrow CH_3CHO + HO_2 \quad (7)$$

Acetaldehyde was not observed in any of the experiments conducted in the absence of NO_x. However, as acetaldehyde is about 8 times more reactive with Cl than ethyl formate [22-24,29,33,34], rapid conversion of this species mainly to CO_2 and CO (via CH_2O), but also to peracetic acid and acetic acid, would be expected. Thus, to first approximation, in the standard NO_x-free experiments conducted here, and using our branching ratio value, reaction (1a) will result in the formation of CO_2 and CO with molar yields of 36±10% and 18±5%, respectively, independent of O_2 partial pressure.

The major focus of this work is related to the products formed from the main site of attack, i.e., at the -CH_2- group, leading to the formation of the $HC(O)OCH(O_2\bullet)CH_3$ radical.

$$Cl + HC(O)OCH_2CH_3 (+ O_2) \rightarrow HC(O)OCH(O_2\bullet)CH_3 + HCl \quad (1b,2b)$$

In the absence of NO_x, this peroxy radical is subsequently converted via reaction with peroxy species to molecular and radical products:

$$HC(O)OCH(O_2\bullet)CH_3 + HO_2 \rightarrow HC(O)OCH(OOH)CH_3 + O_2 \quad (8b)$$

$$HC(O)OCH(O_2\bullet)CH_3 + RO_2 \rightarrow HC(O)OCH(OH)CH_3 + R'CHO + O_2 \quad (5bi)$$

$$\rightarrow HC(O)OC(=O)CH_3 \text{ (AFAn)} + ROH + O_2 \quad (5bii)$$

$$\rightarrow HC(O)OCH(O\bullet)CH_3 + RO\bullet + O_2 \quad (5biii)$$

The alkoxy radical product of reaction (5biii), $HC(O)OCH(O\bullet)CH_3$, may then undergo any of three possible competing reaction pathways, the α-ester rearrangement (9), reaction with O_2 (10), or decomposition via C-C bond scission (11):

$$HC(O)OCH(O\bullet)CH_3 \rightarrow \mathbf{HC(O)OH\ (FA)} + CH_3C(O) \quad (9)$$

$$HC(O)OCH(O\bullet)CH_3 + O_2 \rightarrow \mathbf{HC(O)OC(O)CH_3\ (AFAn)} + HO_2 \quad (10)$$

$$HC(O)OCH(O\bullet)CH_3 \rightarrow \mathbf{HC(O)OC(O)H\ (FAn)} + CH_3 \quad (11)$$

Note that all three stable products, FA, AFAn and FAn, were observed in every experiment conducted, and thus it is at least possible that all three competing $HC(O)OCH(O\bullet)CH_3$ reaction pathways are operative. However, there is evidence to suggest that the observed FAn is not obtained from reaction (11). First, the appearance profile (Figure 1) is curved upwards, in contrast with the linear appearance profiles observed for AFAn and FA. This suggests that a significant fraction of the observed FAn product is not primary, but instead derives from the oxidation of a primary product. Secondly, if the majority of the FAn was obtained from reaction (11), its yield would be expected to decrease with increasing O_2 partial pressure. This is contrary to what is observed - the FAn yield is lowest at low O_2 partial pressure (50 Torr), increases at intermediate O_2, and is essentially independent of O_2 at higher O_2 partial pressures. As discussed further below, it is likely that FAn production results from pathway (1c), rather than (1b). In any event, because the FAn yield is small (<10%), its origin has little effect on the discussion that follows regarding the competition between reactions (9) and (10).

It is clear from Figure 1 and Table 1 that in the absence of NO_x at 298 K, FA and AFAn are the two major organic products obtained from the Cl-atom initiated oxidation of ethyl formate. On average, these two products accounted on a molar basis for (58±4) % of the oxidized ethyl formate, independent of the O_2 partial pressure (50-700 Torr). As

reaction (9) and (10) represent the dominant pathways to formation of FA and AFAn (see further discussion below), it follows that the branching ratio to reaction (1b) is at least 54%. Note that the co-product of formic acid, $CH_3C(O)$, would be expected [34,39,40] to lead to production of CO_2, CO, CH_2O, peracetic acid, CH_3OH and acetic acid, most or all of which are observed.

The competition between reactions (9) and (10) is displayed quantitatively in Figure 2; as expected, the yield of AFAn increases with increasing O_2 partial pressure at the expense of FA. In addition, it is clear that there is a non-zero yield of AFAn at low (zero) O_2 partial pressure. This O_2-independent component of the AFAn production likely originates from reaction of the peroxy radical $HC(O)OCH(O_2\bullet)CH_3$ with itself and other peroxy species, reaction (5b), as discussed earlier. Also, competition between reactions (9) and (10) is expected to lead to a decrease not only in the FA yield with increasing O_2 partial pressure, but also a concomitant decrease in the yields of CO and CO_2. It was observed that the change in the CO yield (from 46% to 34% between 50 and 700 Torr O_2) was roughly equal to the observed change in the FA (39% to 28%) and AFAn (16 to 29%) yields. The observed change in CO_2 yields was measurably higher (96 to 72%), however, for reasons that are not understood at present.

The yield data for FA and AFAn can be used to obtain the rate coefficient ratio k_9/k_{10}. From a consideration of the chemistry, the following relation holds:

$$Y(FA) / [Y(FA) + Y(AFAn)] = C * k_9 / (k_9+k_{10}[O_2]) \qquad (A)$$

where Y(FA) and Y(AFAn) are the fractional molar yields of FA and AFAn, respectively; C is a scaling term that accounts for sources of AFAn other than from reaction (10); k_9 is the first order rate coefficient for reaction (9); and k_{10} is the second-order rate coefficient for reaction (10). Before fitting the data, other sources and losses for FA and AFAn must be considered. As discussed in more detail below, formic acid production is likely to occur as the result of reaction (1c) and subsequent chemistry, particularly at low O_2 partial pressure. Box model simulations of the chemistry, using the Acuchem software package [41], show that this source is small - about 4% and 1% of the formic acid likely originates from (1c) at 50 Torr and 700 Torr O_2, respectively. An additional mechanism for formic acid production is via the reaction of HO_2 with CH_2O [42], and subsequent chemistry of the resultant complex. Again, simulations indicate that

this source is minor, contributing <2% of the observed formic acid at 298 K. To account for these production mechanisms, minor corrections were made to the measured formic acid yields. As alluded to in the experimental section, losses of formic acid and AFAn via reaction with Cl-atoms are negligible, as these species are ≈ 50 and 100 times less reactive with Cl-atoms than is ethyl formate [7,22-24,29,33,34].

A least squares fit of the corrected product yield data to equation (A), shown in Figure 3, leads to a 298 K rate coefficient ratio $k_9/k_{10} = (4.6\pm1.0) \times 10^{19}$ molecule cm^{-3}, with C =0.73 ± 0.05. The reported uncertainty in the rate coefficient ratio is an estimate, and is dominated by possible systematic errors in our understanding of the chemistry rather than by precision errors in spectral analysis. The results indicate that the α-ester rearrangement, reaction (9), is about 9 times more rapid than reaction (10) with O_2 for 1 atm air at 298 K, and will thus dominate the chemistry of $HC(O)OCH(O\bullet)CH_3$ radicals under these conditions. The rate coefficient ratio is in line with expectations - the rate of the α-ester rearrangement process for $HC(O)OCH(O\bullet)CH_3$ is intermediate between the rates for the slower methyl formate and methyl acetate cases and the more rapid ethyl acetate case [5,7,9,11,13-15].

The data are also broadly consistent with those recently reported by Malanca et al. [25]. The majority of their experiments were conducted in the presence of NO_2 (which opens up different alkoxy radical reaction channels), but the results appear to be in semi-quantitative agreement with what is reported here. Malanca et al. [25] report that 62±8% of the reaction occurs at the CH_2 group, in agreement with our findings. In their system, the $HC(O)OCH(O\bullet)CH_3$ radical can undergo not only reactions (9) and (10), but can also react with NO_2 to produce the nitrate species, $HC(O)OCH(ONO_2)CH_3$. Their results show roughly equal (combined) occurrence of the two bimolecular reaction pathways and the α-ester rearrangement in 1 atm O_2, broadly consistent with our findings. (Note that exact comparisons between our data and those of Malanca et al. are not possible as the $[NO_2]$ used in the Malanca et al. study changed over the course of an experiment due to its photolysis, and 2) the conversion of $HC(O)OCH(OO\bullet)CH_3$ to $HC(O)OCH(O\bullet)CH_3$ occurs via its reaction with NO in their work, which opens up the possibility of an influence of chemical activation on the chemistry of the nascent, internally excited $HC(O)OCH(O\bullet)CH_3$ radical [e.g., 7,9,15]). In the absence of NO_2, (i.e., under conditions

similar to our work), Malanca et al. [25] report the formation of formic acid and AFAn in a 2:1 ratio in 1 atm. O_2. This ratio is higher than the roughly 1:1 ratio seen in our study, which may be a consequence of different radical densities in the two studies, and hence the different relative occurrences of various RO_2/RO_2 reactions, which could impact the overall AFAn yield. A more complete summary of rates and barriers for α-ester rearrangement reactions, and the dependencies of these parameters on radical structure, will be presented in a later section.

It remains to consider the reaction of Cl-atoms at the CH_3-group in ethyl formate, which will generate the $HC(O)OCH_2CH_2O_2\bullet$ radical:

$$Cl + HC(O)OCH_2CH_3 \ (+ O_2) \rightarrow \quad HC(O)OCH_2CH_2O_2\bullet \qquad (1c)$$

Note that, given the discussion just presented, the branching to channel (1c) cannot exceed ≈25%. Chemistry associated with this peroxy species will include the following:

$$HC(O)OCH_2CH_2O_2\bullet + RO_2 \rightarrow \quad HC(O)OCH_2CH_2O\bullet + RO + O_2 \qquad (5ci)$$

$$\rightarrow \quad HC(O)OCH_2CH_2OH + R'CHO + O_2 \qquad (5cii)$$

$$\rightarrow \quad HC(O)OCH_2CHO + ROH + O_2 \qquad (5ciii)$$

$$HC(O)OCH_2CH_2O_2\bullet + HO_2 \rightarrow \quad HC(O)OCH_2CH_2OOH + O_2 \qquad (8c)$$

Subsequent reactions of the resulting alkoxy species, $HC(O)OCH_2CH_2O\bullet$, may then include decomposition, isomerization via a 1,5-H atom shift, and/or O_2 reaction:

$$HC(O)OCH_2CH_2O\bullet \rightarrow \quad HC(O)OCH_2\bullet + CH_2O \qquad (12)$$

$$HC(O)OCH_2CH_2O\bullet \rightarrow \quad \bullet C(O)OCH_2CH_2OH \qquad (13)$$

$$HC(O)OCH_2CH_2O\bullet + O_2 \rightarrow \quad HC(O)OCH_2CHO + HO_2 \qquad (14)$$

From previous studies of methyl formate oxidation [9,15], the $HC(O)OCH_2\bullet$ radical product of reaction (12) will, via the $HC(O)OCH_2O\bullet$ species, in part produce FAn and FA:

$$HC(O)OCH_2O\bullet + O_2 \rightarrow \quad HC(O)OCHO \ (FAn) + HO_2 \qquad (15)$$

$$HC(O)OCH_2O\bullet \rightarrow \quad HC(O)OH \ (FA) + HCO \qquad (16)$$

Given the small branching fraction to pathway (1c), our inability to identify species such as $HC(O)OCH_2CHO$ in the IR spectra, and the multiple possible sources of species such as CO, CH_2O and CO_2, it is not possible to draw quantitative conclusions regarding the entire end-product distribution resulting from pathway (1c). Nonetheless, this channel

likely represents the source of FAn in our experiments, as well as a minor source of FA as discussed above with regard to the determination of the rate coefficient ratio k_9/k_{10}. The appearance profile for FAn is curved upwards, suggesting that it is at least in part a secondary product. This behavior may be due to the intermediacy of species such as $HC(O)OCH_2CH_2OH$, $HC(O)OCH_2CHO$ and $HC(O)OCH_2CH_2OOH$, formed from reactions (5c) or (8c) or analogous products formed from $HC(O)OCH_2O_2$ chemistry. Also, we note that the FAn yield is lowest at low O_2 partial pressure (50 Torr), and essentially independent of O_2 at higher O_2 partial pressures as would be expected from competition involving reactions (15) and (16) [9,15].

As a consistency check, a comparison between measured data and a box-model simulation of the chemistry for experiments conducted at 298 K in the presence of 150 Torr O_2 is presented, see Figure 1. Problems in accurately representing the chemistry in the model originate from a lack of quantitative knowledge of the relevant peroxy radical chemistry (e.g., rates and branching in the self-reaction of $HC(O)OCH(OO\bullet)CH_3$), and the subsequent fate of molecular products of this chemistry (e.g., $HC(O)OCH(OOH)CH_3$, etc). In general, measurement-model agreement was best when molecular channels of RO_2-RO_2 reactions were kept low. In the comparison shown, branching ratios of 10% to molecular channels were assumed. For reactions involving either HO_2 or acyl peroxy radicals, total rate coefficients of 10^{-11} cm^3 $molecule^{-1}$ s^{-1} were used while for all other RO_2/ RO_2 reactions, total rate coefficients of 10^{-12} cm^3 $molecule^{-1}$ s^{-1} were assumed. Despite the obvious limitations, there is generally good agreement between the measured and modeled concentrations of the major products. The most obvious model-measurement disagreements involve CO_2, where the measurements are higher than the model, and AFAn, where the reverse is true. Spurious production of CO_2 is often observed upon irradiation of the chamber, and may contribute to the observed disagreement. In the case of AFAn, a major source of this species in the model is from the formation and subsequent destruction of $HC(O)OCH(OOH)CH_3$,

$$HC(O)OCH(OO\bullet)CH_3 + HO_2 \rightarrow HC(O)OCH(OOH)CH_3 + O_2 \qquad (8b)$$

$$Cl + HC(O)OCH(OOH)CH_3 \rightarrow \rightarrow HC(O)OC(O)CH_3$$

Loss of this species via other routes (possibly heterogeneous) in the chamber could contribute to the model-measurement discrepancy.

As a possible solution to some of the measurement-model discrepancies noted above, an anonymous reviewer pointed out the possibility of an additional channel in the chemistry of the $HC(O)OCH(O\bullet)CH_3$, a unimolecular 1,4-H shift show below:

$$HC(O)OCH(O\bullet)CH_3 \rightarrow \bullet C(O)OCH(OH)CH_3,$$

which would lead to CO_2 and CH_3CHO as likely end-products. While we cannot rule out the occurrence of this channel altogether, a re-examination of our yield data (in particular, the formic acid data and its dependence on O_2 partial pressure) indicates that this can at most be a minor channel - we estimate a maximum occurrence of 25% relative to the α-ester reaction, which would lead to a concomitant 25% increase in our reported k_9/k_{10} ratios. To conclude this section, we note that Sellevåg and Nielsen [29] also reported upon a brief study of the Cl-initiated oxidation of ethyl formate in air. Major products observed were FA, CO and CO_2, consistent with our findings. However, these authors postulated that these species are formed following Cl-atom attack at the methyl group, inconsistent with the interpretation presented here and in [25] and with the now well-established occurrence of the α-ester rearrangement.

2) Ethyl Formate vs. Temperature: Chemistry of the $HC(O)OCH(O\bullet)CH_3$ radical

The oxidation of ethyl formate was also studied above (325 K) and below (273 and 255 K) ambient temperature. At 325 K, products observed were FA, AFAn, CO, CO_2, peracetic acid, FAn, and possibly trace amounts of CH_2O in some cases. In general, yields were similar to those found at 298 K; however, unlike room temperature, yields of most products (e.g., CO, 44±4%; FA, 45±3%; AFAn, 12±2%; peracetic acid, ≈6%) were found to be independent of O_2 partial pressure. Yields of CO_2 were in the range 80-100%, with a possible (weak) inverse correlation with O_2 partial pressure. The only species showing a distinct dependence on O_2 partial pressure was FAn, whose yield increased from about 1.5-2% in the presence of 50 Torr O_2 to about 5% in 700 Torr O_2.

This independence of the yields of the main products on O_2 partial pressure is attributed to the rapidity of the α-ester rearrangement at elevated temperature. The only significant source of AFAn under these conditions is from molecular channels of reactions involving $HC(O)OCH(O_2\bullet)CH_3$ with peroxy species, while essentially all $HC(O)OCH(O\bullet)CH_3$ radicals are converted to FA via reaction (9), even at high O_2 partial

pressure. As was the case at 298 K, the dependence of the FAn yield on O_2 partial pressure is consistent with competition between reactions (15) and (16), k_{16}/k_{15} = (4.8±0.7) x 10^{18} molecule cm^{-3} at 324 K [15]. Simulations indicated that the formation of FA via reaction of HO_2 with CH_2O was not significant at this temperature, due to rapid decomposition of the HO_2/CH_2O adduct [42].

While the negligible variation of the FA/AFAn ratio on O_2 partial pressure does not allow for an accurate, independent determination of k_9/k_{10} at 325 K, examination of the observed product ratio vs. O_2 partial pressure data allows us to conclude that k_9/k_{10} > 1.4 x 10^{20} molecule cm^{-3}. A global fit to the entire dataset, presented in detail below, gives k_9/k_{10} = 2.0 x 10^{20} molecule cm^{-3}, consistent with this lower limit.

Products observed at low temperature (273 and 255 K) were FA, AFAn, CO, and CO_2, while FAn and trace amounts of CH_2O were also observed at 273 K. These products typically accounted for 65-70% of the reacted ethyl formate. As is evident from Table 1, yields of most products showed a strong correlation with O_2 partial pressure: AFAn formation was favored at high O_2 at the expense of FA, CO, and CO_2, consistent with competition between reactions (9) and (10). The FAn yield (≈6%), however, was independent of O_2, consistent with its formation from attack at the CH_3-group in ethyl formate (e.g., reactions 1c, 5ci, 12, and 15). Note that, at reduced temperature, reaction (15) is strongly favored over reaction (16) even at 50 Torr O_2 [15]. This observed independence of the FAn yield on O_2 is strong evidence for negligible formation of FA from reaction (16) at reduced temperature.

Before using the O_2 dependence of the FA and AFAn yields to determine k_9/k_{10} values at reduced temperature, FA formation from HO_2 / CH_2O adduct chemistry was first accounted for. Box model simulations of the reaction system indicated that ≈10% (≈25%) of the observed FA was originating from this chemistry at 273 (255) K. After correction, it was found that the sum of the FA and AFAn yields was essentially independent of temperature, an indication that the magnitude of the correction applied is reasonable. Note also that the determination of k_9/k_{10} ratios is not overly sensitive to this correction, as the FA concentration appears in both the numerator and denominator in Equation (A) and the applied correction is independent of $[O_2]$. The corrected yield data are shown in Figure 3. Fits to the data (at each temperature, independently) yielded:

$k_9/k_{10} = (1.53\pm0.35) \times 10^{19}$ molecule cm^{-3} at 273 K, and $(0.42\pm0.14) \times 10^{19}$ molecule cm^{-3} at 255 K.

Lastly, a least squares fit was conducted to the entire data set (i.e., the data obtained at all temperatures studied). Here, the rate coefficient ratio k_9/k_{10} was represented in the fit by two parameters, i.e., $k_9/k_{10} = A \exp(-B/T)$, while the scaling factor C was determined independently at each temperature. This global fit yielded $k_9/k_{10} = 1.8 \times 10^{26} \exp(-4466/T)$ molecule cm^{-3}. Rate coefficient ratios obtained from fits to the individual temperatures, as well as those obtained from the global fit are given in Table 2; very good agreement is seen between the two sets of data. Comparisons of these data with rate data on the α-ester rearrangement in other esters will be made in a later section.

3) Ethyl Acetate at 298 K

Products observed from the Cl-atom initiated oxidation of ethyl acetate at 298 K were acetic acid (AA), acetic acid anhydride (AAn), CO, CO_2, CH_2O, and possibly traces of peracetic acid and acetic formic anhydride (AFAn). The identified products accounted for, on average, 75±15% of the reacted ethyl acetate, on a carbon atom basis. Additional absorption features at 940, 1040, 1075, 1122, 1200, 1230, 1255, 1337, 1381, 1444, 1742 and 1790 cm^{-1} were also noted, and are likely associated with stable end-products of RO_2/RO_2 and RO_2/HO_2 chemistry, such as $CH_3C(O)OCH(OOH)CH_3$, or $CH_3C(O)OCH(OH)CH_3$.

Results from a typical experiment (conducted in 150 Torr O_2, at a total pressure of 750 Torr) are shown in Figure 4. Appearance profiles of AA, AAn, and CO_2 appear linear, indicating the likelihood that these are primary products of the ethyl acetate oxidation. Evidence for conversion of CH_2O (appearance profile curved downward) to CO (appearance profile curved upward) is seen in the data, as expected given the high relative reactivity of formaldehyde with Cl-atoms ($k_{Cl+CH2O} / k_{Cl+CH3C(O)OCH2CH3} \approx 4$) [33-36].

Yields of the product species were found to be noticeably (but weakly) dependent on O_2 partial pressure, see the summary in Table 3, with the yield of AAn increasing with increasing O_2 partial pressure at the expense of the other species (AA, CO_2, and possibly

the sum of CO + CH_2O). Similar to the ethyl formate study described above, and as presented in quantitative detail below, the source of this O_2 dependence stems from a competition between the α-ester rearrangement (R20) of the $CH_3C(O)OCH(O\bullet)CH_3$ radical and its reaction (21) with O_2:

$$Cl + CH_3C(O)OCH_2CH_3 \rightarrow CH_3C(O)OCH\bullet CH_3 + HCl \quad (17a)$$

$$CH_3C(O)OCH\bullet CH_3 + O_2 \rightarrow CH_3C(O)OCH(OO\bullet)CH_3 \quad (18)$$

$$CH_3C(O)OCH(OO\bullet)CH_3 + RO_2 \rightarrow CH_3C(O)OCH(O\bullet)CH_3 + RO\bullet + O_2 \quad (19)$$

$$CH_3C(O)OCH(O\bullet)CH_3 \rightarrow CH_3C(O)OH + CH_3C(O) \quad (20)$$

$$CH_3C(O)OCH(O\bullet)CH_3 + O_2 \rightarrow CH_3C(O)OC(O)CH_3 \text{ (AAn)} + HO_2 \quad (21)$$

The sum of the AAn and AA yields was determined to be 79±5%, independent of O_2 partial pressure, implying that at least 74% of the reaction of Cl-atoms with ethyl acetate proceeds via abstraction from the $-CH_2-$ group (assuming no other sources of these end products exists, an assumption that is verified below). Given the possibility of the conversion of $CH_3C(O)OCH(OO\bullet)CH_3$ to other stable products [*e.g.*, $CH_3C(O)OCH(OH)CH_3$ and $CH_3C(O)OCH(OOH)CH_3$], it is then possible that the branching ratio to reaction (17a) is considerably greater than 74%.

Before using the AA and AAn product yield data to assess the magnitude of the rate coefficient ratio k_{20}/k_{21}, it is important to consider other potential sources and sinks for these product species. Reaction of Cl-atoms with AA is about 650 times slower than reaction with ethyl acetate [33-36]. The reaction of Cl with AAn has not been measured, but is anticipated to be similar in magnitude to that for AA. Thus, losses of either product via this route are negligible.

In addition to its formation via reaction (21), AAn may also form via molecular channels of $CH_3C(O)OCH(OO\bullet)CH_3$ chemistry, e.g.,

$$2\ CH_3C(O)OCH(OO\bullet)CH_3 \rightarrow CH_3C(O)OCH(OH)CH_3 + AAn + O_2$$

$$CH_3C(O)OCH(OO\bullet)CH_3 + HO_2 \rightarrow CH_3C(O)OCH(OOH)CH_3 + O_2$$

$$Cl + CH_3C(O)OCH(OH)CH_3\ (+ O_2) \rightarrow AAn + HO_2 + HCl$$

$$Cl + CH_3C(O)OCH(OOH)CH_3 \rightarrow AAn + OH + HCl$$

These O_2-independent channels will be accounted for in the analysis below. Additional sources of AA also exist. For example, the co-product of AA in reaction (20) is $CH_3C(O)$, itself a possible source of additional AA [34,39,40]:

$$CH_3C(O) + O_2 \rightarrow CH_3C(O)O_2$$

$$CH_3C(O)O_2 + CH_3C(O)O_2 \rightarrow 2\,(CH_3 + CO_2) + O_2$$

$$CH_3C(O)O_2 + RO_2 \rightarrow CH_3 + CO_2 + O_2 + RO$$

$$CH_3C(O)O_2 + HO_2 \rightarrow CH_3 + CO_2 + O_2 + OH \quad (40\%)$$

$$\rightarrow CH_3C(O)OH + O_3 \quad (15\%)$$

$$\rightarrow CH_3C(O)OOH + O_2 \quad (45\%)$$

However, no peracetic acid was conclusively detected in any of the 298 K ethyl acetate experiments carried out (yield < 10%) and thus it is unlikely that any significant acetic acid production occurred via this mechanism.

The possible formation of acetic acid from Cl-atom reaction with ethyl acetate at sites other than the CH_2 group must also be considered. On the basis of mechanistic data regarding the reaction of Cl with AA and methyl acetate [7,15,34], reaction at the acetate group probably contributes less than 1% to the overall reaction of Cl-atoms with ethyl acetate. Given the product yields discussed above, it is then possible that a measurable (≤25%) fraction of the reactivity occurs at the CH_3 end of the ethyl fragment:

$$Cl + CH_3C(O)OCH_2CH_3 \rightarrow CH_3C(O)OCH_2CH_2\bullet + HCl \quad (17b)$$

$$CH_3C(O)OCH_2CH_2\bullet + O_2 \rightarrow CH_3C(O)OCH_2CH_2OO\bullet$$

$$CH_3C(O)OCH_2CH_2OO\bullet + RO_2 \rightarrow CH_3C(O)OCH_2CH_2O\bullet + RO + O_2$$

Likely fates of the resultant alkoxy species, $CH_3C(O)OCH_2CH_2O\bullet$, include reaction with O_2, or decomposition:

$$CH_3C(O)OCH_2CH_2O\bullet + O_2 \rightarrow CH_3C(O)OCH_2CHO + HO_2$$

$$CH_3C(O)OCH_2CH_2O\bullet \rightarrow CH_3C(O)OCH_2\bullet + CH_2O$$

In either case, the possibility for formation of $CH_3C(O)OCH_2O\bullet$ radicals, and hence AA, must be considered [7,15]:

$$CH_3C(O)OCH_2O\bullet + O_2 \rightarrow CH_3C(O)OC(O)H\ (AFAn) + HO_2 \quad (22)$$

$$CH_3C(O)OCH_2O\bullet \rightarrow CH_3C(O)OH + HCO \quad (23)$$

$$HCO + O_2 \rightarrow HO_2 + CO$$

Previous studies of methyl acetate oxidation [7,15] show that reactions (22) and (23) are competitive at 298 K, and occur with essentially equal rates in 1 atm. air. However, given that AFAn could not be conclusively identified in any of the 298 K ethyl acetate experiments conducted (yield < 5% even at high O_2 partial pressures), it can be concluded that this route provides at most a very minor source of AA.

It is thus apparent that the observed AFAn and AA product yields can be used to determine k_{20}/k_{21}, as follows:

$$Y(AA) / [Y(AA) + Y(AAn)] = D * k_{20}/(k_{20}+k_{21}[O_2]) \qquad (B)$$

where Y(AA) and Y(AAn) are the fractional molar yields of AA and AAn, respectively; D is a scaling term that accounts for sources of AAn other than from reaction (21); k_{20} is the first order rate coefficient for reaction (20); and k_{21} is the second-order rate coefficient for reaction (21). Least-squares fitting of the data measured at 298 K to this expression yields $k_{20}/k_{21} = 1.2 \times 10^{20}$ molecule cm^{-3}, with D = 0.72, see Figure 5. On the basis of test fits conducted with product yields varied over ranges determined by precision and possible systematic errors, the uncertainty on the retrieved rate coefficient ratio is estimated to be ±50%. The relatively large magnitude of the uncertainty is due largely to the fact that there is only a weak change in the product yields with O_2 partial pressure. Despite the inherent uncertainty in the measured rate coefficient ratio, it is apparent that the α-ester rearrangement will dominate the chemistry of $CH_3C(O)OCH(O\bullet)CH_3$ at 298 K, occurring about 24 times more rapidly than its reaction with O_2 in 1 atm. air. This result confirms earlier laboratory and theoretical findings [5,11,13]. Tuazon et al. [5], in their initial discovery of the α-ester process, found a 96±8% yield of AA and a < 5% yield of AAn in the OH-initiated oxidation ethyl acetate in 1 atm. air at 298 K, entirely consistent with the 96% : 4% ratio predicted by our rate coefficient ratio. In a similar OH-initiated experiment, Picquet-Varrault et al. [11] also found a high ratio of AA (75±13%) to AAn (2±1%), but also reported the formation of measurable (15±5% yield) amounts of acetoxyacetaldehyde, $CH_3C(O)OCH_2CHO$. More general conclusions regarding the rate of the α-ester rearrrangement for a range of radicals of the form RC(O)OCH(O•)R, including comparisons with theoretical studies [13,14], are made below.

4) Ethyl Acetate Oxidation as a function of Temperature

Ethyl acetate oxidation experiments were also carried out at temperatures above (325 K) and below (273 and 249 K) ambient, over a range of O_2 partial pressures (50-700 Torr). At all temperatures studied, observed products (AA, AAn, CO, CO_2, lesser amounts of CH_2O, AFAn and possibly peracetic acid) and mass balances (75-85%) were very similar to those seen at 298 K.

At 325 K, the sum of the yields of AA and AAn was determined to be 81±5%, independent of O_2. The AAn to AA product yield ratio increased very slightly with increasing O_2 partial pressure, see Table 3, while CO and CO_2 yields showed no discernable O_2 dependence. Fits of the observed AA and AAn yield data to equation (B), shown in Figure 5, yielded $k_{20}/k_{21} = 3.5 \times 10^{20}$ molecule cm^{-3}. Uncertainties on this ratio are quite large however, due to the weak dependence of the product ratio on O_2 partial pressure over the accessible range, and a more conservative estimate of $k_{20}/k_{21} > 1.5 \times 10^{20}$ molecule cm^{-3} is presented on the basis of the 325 K data alone.

Product yields at reduced temperature (summarized in Table 3) showed a more pronounced dependence on O_2 partial pressure (again with AAn increasing with increasing O_2 partial pressure at the expense of AA, CO and CO_2), owing to the slower rate of occurrence of the α-ester rearrangement and thus a closer competition between this rearrangement and the O_2 reaction (21). On the basis of low (or undetectable) yields of AFAn and peracetic acid in these low temperature studies, production of AA either from chemistry of the $CH_3CO\bullet$ product of the α-ester rearrangement or from chemistry of the $CH_3C(O)OCH_2O\bullet$ radical is deemed negligible. Fitting of the measured AA and AAn yields at each individual temperature to Equation (B), as shown in Figure 5, yielded $k_{20}/k_{21} = (5.3\pm2.0) \times 10^{19}$ molecule cm^{-3} at 273 K, and $k_{20}/k_{21} = (2.1\pm0.7) \times 10^{19}$ molecule cm^{-3} at 249 K.

A fit of the entire ethyl acetate dataset (i.e., data obtained at all temperatures) to Equation (B) was also carried out, see Table 4. Here, the rate coefficient ratio k_{20}/k_{21} was expressed in Arrhenius form, $k_{20}/k_{21} = A \exp(-B/T)$, with *A* and *B* as fit parameters, while the scaling factor, D, at each temperature was fit independently. Best fit, as shown by the dashed curves in Figure 5, was obtained with $k_{20}/k_{21} = 1.4 \times 10^{24} \exp(-2765/T)$ molecule cm^{-3}. However, it was found that very reasonable fits could also be obtained for a fairly

wide range of values of A (≈[0.4-10] × 10^{24}) and B (≈2400-3300 K), with the two variables strongly correlated. For all reasonable fits, retrieved rate coefficients at reduced temperature remained tightly constrained, k_{20}/k_{21} = (1.9-2.2) × 10^{19} molecule cm^{-3} at 249 K and k_{20}/k_{21} = (5.1-6.2) × 10^{19} molecule cm^{-3} at 273 K. However, more substantial variation was seen in the retrieved rate coefficient ratios at elevated temperatures - in essence, the yield data at 298 K and above do not vary sufficiently with O_2 partial pressure to constrain the overall fit.

Including the work presented here, there are now T-dependent data [15] for the rate of occurrence of the α-ester rearrangement (relative to reaction with O_2) for four radicals, those of formula RC(O)OCHR′O•, R and R′ = H or CH_3. The four sets of measurements are summarized in Figure 6. Generally, an increase in the rate of the α-ester rearrangement relative to O_2 reaction is seen upon substitution of CH_3 for H. Near 298 K, the rearrangement occurs 3-4 times faster for the acetate than for the corresponding formate, while substitution of an ethyl for a methyl group in the parent ester leads to roughly a factor of 30 increase. Because of uncertainties in the measurements and because the data span a fairly narrow temperature range, however, trends in A-factors and energy barriers with structure are not readily apparent from the data. However, on the basis of other alkoxy radical reactions (e.g., thermal decomposition and isomerization) [43,44], it seems reasonable to assume that A-factors for the set of α-ester rearrangements are more or less independent of molecular structure, and that changes in rate are mostly associated with changes in the activation energy. Thus, a fit of the data for all species was conducted, excluding the 325 K data points from ethyl acetate and ethyl formate (which are too high to be accurately determined), with the A-factor ratio fixed to a constant value for all four reactions and the activation energy for each compound determined as a fit parameter. Best fit, shown in Figure 6, was obtained for $A_{\alpha\text{-ester}} / A_{O2}$ = 3.3 × 10^{25} molecule cm^{-3}, and activation energy differences of about 10.0, 9.2, 8.0, and 7.2 kcal/mole for methyl formate, methyl acetate, ethyl formate, and ethyl acetate, respectively. Given that typical activation energies for reaction of small alkoxy radicals with O_2 fall in the range 0-1 kcal/mole [43,44], barriers of about 10.5±1.5, 9.7±1.5, 8.4±1.5, and 7.7±1.5 are then estimated for the four species. These barriers are comparable to data obtained in theoretical treatments. Ferenac et al. [14]

estimate a barrier height of 8-12 kcal/mole for the methyl acetate system, while Rayez et al. [13] reported a barrier of 6.5 kcal/mole for ethyl acetate, a little lower than what is implied by our data. A theoretical treatment of the $HC(O)OCH(O\bullet)CH_3$ radical has also been conducted as part of our recent study [38] of isopropyl and t-butyl formate oxidation. In that work, the α-ester rearrangement reaction (9) and decomposition reaction (11) were found to be competitive, with the α-ester process possessing an activation barrier of 12 kcal/mole, somewhat higher than measured here.

Summary

Rates of the α-ester rearrangement reaction have been determined for the $HC(O)OCH(O\bullet)CH_3$ and $CH_3C(O)OCH(O\bullet)CH_3$ alkoxy species, relative to reaction of these radicals with O_2. For both species, the rearrangement reaction is found to dominate over reaction with O_2 in 1 atm. air at 298 K, and to be competitive with the O_2 reaction near 250 K. Barriers to the rearrangement reaction of 8.4±1.5 and 7.7±1.5 kcal/mole are estimated for the two radicals. In considering data for the four structurally similar radicals (this work and [15]), $RC(O)OCH(O\bullet)R'$, R,R′ = H,CH_3, it is seen that the rates of the rearrangement reaction near 298 K increase by a factor of ≈3-4 upon substitution of R=CH_3 for R=H and a factor of ≈30 upon substitution of R′=CH_3 for R′=H, corresponding to decreases in the barrier height of ≈1 and 2 kcal/mole, respectively.

Acknowledgments

The National Center for Atmospheric Research is operated by the University Corporation for Atmospheric Research, under the sponsorship of the National Science Foundation. This work was funded in part by the NASA ROSES (Atmospheric Composition) program. Thanks are due to Louisa Emmons and Doug Kinnison of NCAR for their careful reading of the manuscript, to G. Argüello and F. Malanca (Universidad Nacional de Córdoba, Argentina) for helpful conversations and for kindly providing their EoPAN cross section data, and to two anonymous reviewers for their helpful comments.

References :

1. Passant, N. R.; Richardson, S. J.; Swannell, R. P. J.; Gibson, N.; Woodfield, M. J.; van der Lugt, J. P.; Wolsink, J. H.; Hesselink, P. G. M. Atmos Environ 1993, 16, 2555.

2. Wallington, T. J.; Dagaut, P.; Liu, R.; Kurylo, M. J. Int J Chem Kinet 1988, 20, 177.

3. El Boudali, A.; Le Calvé, S.; Le Bras, G.; Mellouki, A. J Phys Chem 1996, 100, 12364.

4. Le Calvé, S.; Le Bras, G.; Mellouki, A. J Phys Chem A 1997, 101, 5489.

5. Tuazon, E. C.; Aschmann, S. M.; Atkinson, R; Carter, W. P. L. J Phys Chem A 1998, 102, 2316.

6. Good, D. A.; Francisco, J. S. J. Phys Chem A 2000, 104, 1171.

7. Christensen, L. K.; Ball, J. C.; Wallington, T. J. J Phys Chem A 2000, 104, 345.

8. Cavalli, F.; Barnes, I.; Becker, K. H.; Wallington, T. J. J. Phys Chem A, 2000, 104, 11310.

9. Wallington, T. J.; Hurley, M. D.; Maurer, T.; Barnes, I.; Becker, K. H.; Tyndall, G. S.; Orlando, J. J.; Pimentel, A. S.; Bilde, M. J Phys Chem A 2001, 105, 5146.

10. Wallington, T. J.; Ninomiya, Y.; Mashino, M.; Kawasaki, M.; Orkin, V. L.; Huie, R. E.; Kurylo, M. J.; Carter, W. P. L.; Luo, D.; Malkina, I. L. J Phys Chem A 2001, 105, 7225.

11. Picquet-Varrault, B.; Doussin, J. F.; Durand-Jolibois, R.; Carlier, P. Phys Chem Chem Phys 2001, 3, 2595.

12. Picquet-Varrault, B.; Doussin, J. F.; Durand-Jolibois, R.; Carlier, P. J. Phys. Chem. A 2002, 106, 2895.

13. Rayez, M. T.; Picquet-Varrault, B.; Caralp, F.; Rayez, J. C. Phys Chem Chem Phys 2002, 4, 5789.

14. Ferenac, M. A.; Davis, A. J.; Holloway, A. S.; Dibble, T. S. J Phys Chem A 2003, 107, 63.

15. Tyndall, G. S.; Pimentel, A.S.; Orlando, J.J. J Phys Chem A 2004, 108, 6850.

16. Wallington, T. J.; Japar, S. M. Environ Sci Technol 1991, 25, 410.

17. Wallington, T. J.; Andino, J. M.; Potts, A. R.; Rudy, S. J.; Siegl, W. O.; Zhang, Z.; Kurylo, M. J.; Huie, R. E. Environ Sci Technol 1993, 27, 98.

18. Eberhard, J.; Muller, C.; Stocker, D. W.; Kerr, J. A. Int J Chem Kinet 1993, 25, 639.

19. Smith, D. F.; McIver, C. D.; Kleindienst, T. E. Int J Chem Kinet 1995, 27, 453.

20. Cheema, S. A.; Holbrook, K. A.; Oldershaw, G. A.; Starkey, D. P.; Walker, R. W. Phys Chem Chem Phys 1999, 1, 3243.

21. Andreae, M.; Merlet, P. Global Biogeochemical Cycles 2001, 15, 955.

22. Wallington, T. J.; Hurley, M. D.; Harvanto, A. Chem Phys Lett 2006, 432, 57.

23. Ide, T.; Iwasaki, E.; Matsumi, Y.; Xing, J.-H.; Takahashi, K.; Wallington, T. J. Chem Phys Lett, 2008, 467, 70.

24. Bravo, I.; Aranda, A.; Diaz-deMera, Y.; Moreno, E.; Tucceri, M. E.; Rodriguez, D. Phys Chem Chem Phys 2009, 11, 384.

25. Malanca, F.; Fraire, J. C.; Argüello, G. A. J Photochem Photobiol A: Chem 2009, 204, 75.

26. Szilagyi, I.; Dobe, S.; Berces, T., Marta, F. Z Physik Chemie 2004, 218, 479-492.

27. Picquet, B.; Heroux, S.; Chebbi, A. ; Doussin, J.-F.; Durand-Holibois, R.; Monod, A.; Loirat, H.; Carlier, P. Int J Chem Kinet 1998, 30, 839.

28. Carter, W. P. L.; Documentation of the SAPRC-99 chemical mechanism for VOC reactivity assessment, Final Report to California Air Resources Board Contract No. 92-329, and (in part) 95-308, 2000. Available at http://pah.cert.ucr.edu/~carter/

29. Sellevåg, S. R. ; Nielsen, C. J. Asian Chem Lett 2003, 7, 15.

30. Atkinson, R. Atmos Environ 2000, 34, 2063.

31. Orlando, J.J. Phys Chem Chem Phys 2007, 9, 4189-4199.

32. Shetter, R. E.; Davidson, J. A.; Cantrell, C. A.; Calvert, J. G. Rev Sci Instrum 1987, 58, 1427.

33. Notario, A.; Le Bras, G.; Mellouki, A. J Phys Chem A 1998, 102, 3112.

34. Atkinson, R; Baulch, D. L.; Cox, R. A.; Crowley, J. N.; Hampson, R. F.; Kerr, J. A.; Rossi, M. J.; Troe, J. IUPAC subcommittee for gas kinetic data evaluation, *www.iupac-kinetic.ch.cam.ac.uk.*

35. Cuevas, C.A.; Notario, A.; Martinez, E.; Albaladejo, J. Atmos Environ 2005, 39, 5091.

36. Xing, J.-H.; Takahashi, K.; Hurley, M. D.; Wallington, T. J. Chem Phys Lett 2009, 474, 268.

37. Christensen, L.; Wallington, T. J.; Guschin, A.; Hurley, M. D. J Phys Chem A 1999, 103, 4202.

38. Pimentel, A. S.; Tyndall, G. S.; Orlando, J. J.; Hurley, M. D.; Wallington, T. J.; Sulbaek Andersen, M. P.; Marshall, P.; Dibble, T. S., accompanying paper submitted to Int J Chem Kinet.

39. Orlando, J. J.; Tyndall, G. S.; Vereecken, L.; Peeters, J. J Phys Chem A 2000, 104, 11578.

40. Hasson, A.; Tyndall, G. S.; Orlando, J. J. J Phys Chem A 2004, 108, 5979.

41. Braun, W.; Herron, J. T.; Kahaner, D. K. Int J Chem Kinet 1988, 20, 51.

42. Veyret, B.; Rayez, J. C.; Lesclaux, R. J Phys Chem 1982, 86, 3424.

43. Atkinson, R. Int J Chem Kinet 1997, 29, 99.

44. Orlando, J. J.; Tyndall G. S.; Wallington, T. J. Chem Rev 2003, 103, 4657

Table 1: Observed (uncorrected) product yields (% of ethyl formate consumed, on a per mole basis) as a function of O_2 partial pressure from the Cl-atom initiated oxidation of ethyl formate at a total pressure of 730±30 Torr. Results shown are from the average of multiple experiments at each O_2 partial pressure. Uncertainties shown at the top of each column apply to all data in that column.

	298 K					273 K			255 K	
P(O_2)	**CO_2**	**CO**	**FA**	**AFAn**	**FAn**	**FA**	**AFAn**	**FAn**	**FA**	**AFAn**
30									38±4	27±3
50	97±7	46±5	39±4	16±3	4±2	29±4	18±3	5±2	31	30
150	90	42	39	19	7	24	26	6	21	39
300	84	35	38	22	7	23	33	6	16	51
500	78	38	31	26	7	19	37	6	11	50
700	72	34	28	29	7	14	37	6		

Table 2: Rate coefficient ratios k_9 / k_{10} obtained from fits of FA and AFAn yield data to Equation (A). Ratios shown are from fits to the data from each temperature individually, or from a global fit to the complete dataset; see text for details.

Temp. (K)	**k_9/k_{10} (molecule cm^{-3}) - from separate fits to data at each T**	**k_9/k_{10} (molecule cm^{-3}) - from global fit to entire dataset**
325	$> 14 \times 10^{19}$	$(20\pm7) \times 10^{19}$
298	$(4.6\pm1.0) \times 10^{19}$	$(5.5\pm1.0) \times 10^{19}$
273	$(1.53\pm0.4) \times 10^{19}$	$(1.4\pm0.4) \times 10^{19}$
255	$(0.42\pm0.14) \times 10^{19}$	$(0.44\pm0.14) \times 10^{19}$

Table 3: Observed (uncorrected) product yields (% of ethyl acetate consumed, on a per mole basis) as a function of O_2 partial pressure from the Cl-atom initiated oxidation of ethyl acetate at a total pressure of 730±30 Torr. Results shown are from the average of multiple experiments at each O_2 partial pressure. Uncertainties shown at the top of each column apply to all data in that column.

	325 K		298 K			273 K		249 K	
$P(O_2)$	**AA**	**AAn**	**CO_2**	**AA**	**AAn**	**AA**	**AAn**	**AA**	**AAn**
50	64±4	18±3	65±6	55±4	21±3	56±4	29±3	50±4	33±3
50								50	35
150	66	20	64	53	26	47	30	42	43
150						48	31	39	44
300	63	19	64	52	26	49	35	32	48
400	61	19						31	54
500	57	18	55	48	30	41	43	25	53
700	60	22	51	52	32	35	40	26	61
700								22	55

Table 4: Rate coefficient ratios k_{20} / k_{21} obtained from fits of AA and AAn yield data to Equation (B). Ratios shown are from fits to the data from each temperature individually, or from a global fit to the complete dataset; see text for details.

Temp. (K)	**k_{20}/k_{21} (molecule cm^{-3}) - from separate fits to data at each T**	**k_{20}/k_{21} (molecule cm^{-3}) - from global fit to entire dataset**
325	$> 15 \times 10^{19}$	$(28\pm15) \times 10^{19}$
298	$(12\pm6) \times 10^{19}$	$(13\pm6) \times 10^{19}$
273	$(5.3\pm2.0) \times 10^{19}$	$(5.4\pm2.0) \times 10^{19}$
249	$(2.1\pm0.7) \times 10^{19}$	$(2.1\pm0.7) \times 10^{19}$

Figure 1: Observed (uncorrected) product concentrations versus consumption of ethyl formate following photolysis of mixtures of Cl_2 and ethyl formate in 720 Torr synthetic air at 298 K. Symbols represent measured product concentrations, while lines represent results from a box-model simulation; see text for details.

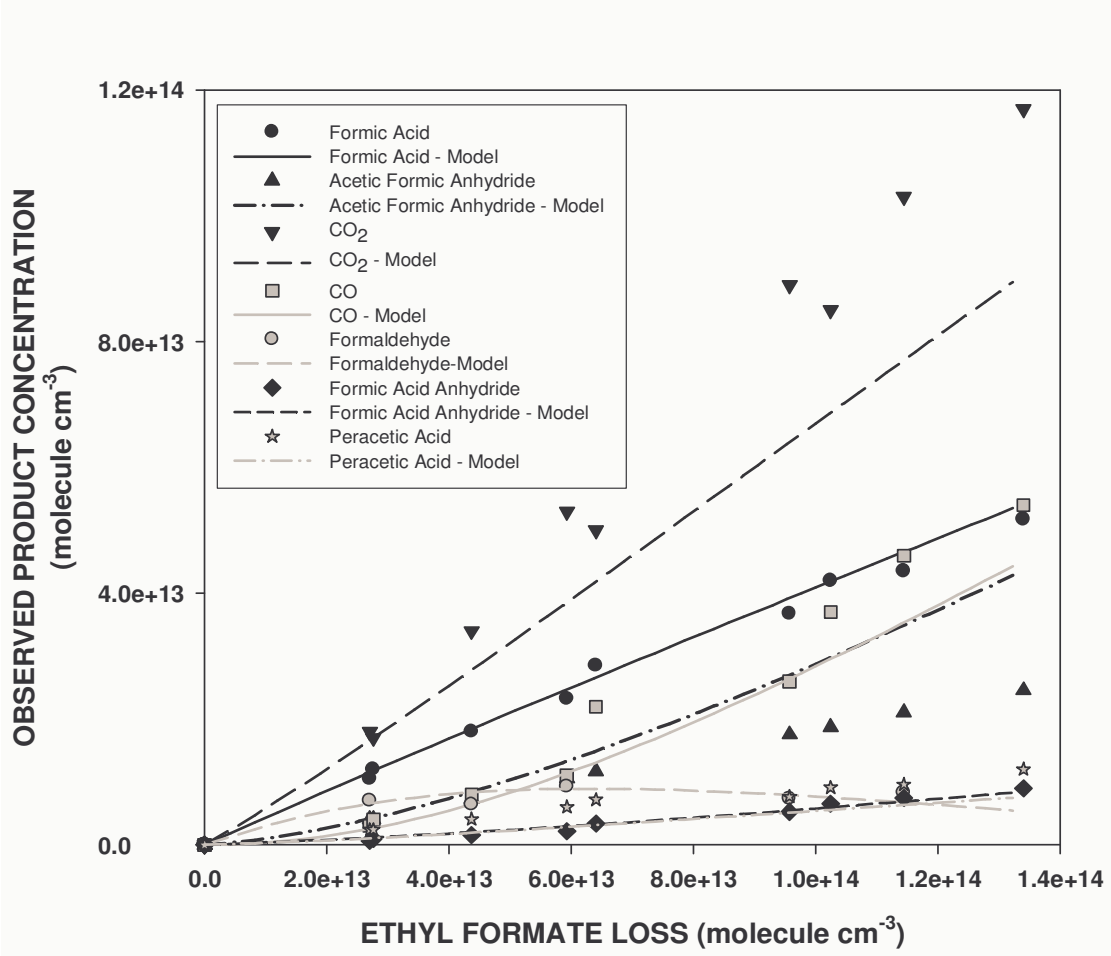

Figure 2: Fractional molar yields of formic acid (triangles) and acetic formic anhydride (AFAn, circles) as a function of O_2 partial pressure at 298 K, obtained from the photolysis of Cl_2 /ethyl formate / O_2 / N_2 mixtures. Solid lines represent fits of the data to Equation (A), which yielded $k_9/k_{10} = 4.6 \times 10^{19}$ molecule cm^{-3}, C = 0.73, see text for details.

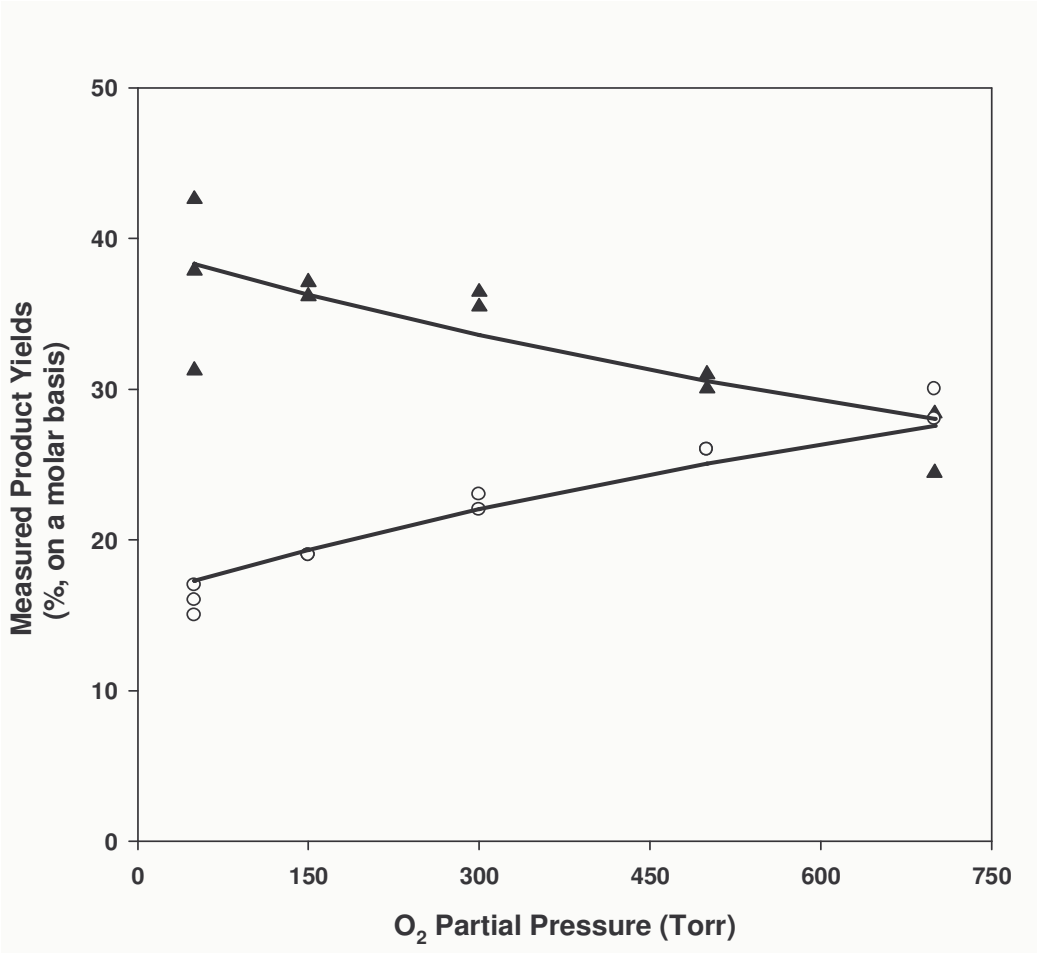

Figure 3: Product yield data { Y(FA) / [Y(FA) + Y(AFAn)] } obtained from Cl-atom initiated oxidation of ethyl formate as a function of O_2 partial pressure. Symbols represent measured data – solid circles 325 K; open triangles, 298 K; solid squares, 273 K; open triangles, 255 K. Solid lines are fits to the data at each individual temperature, dashed lines are results of a fit to the entire dataset, see text for details.

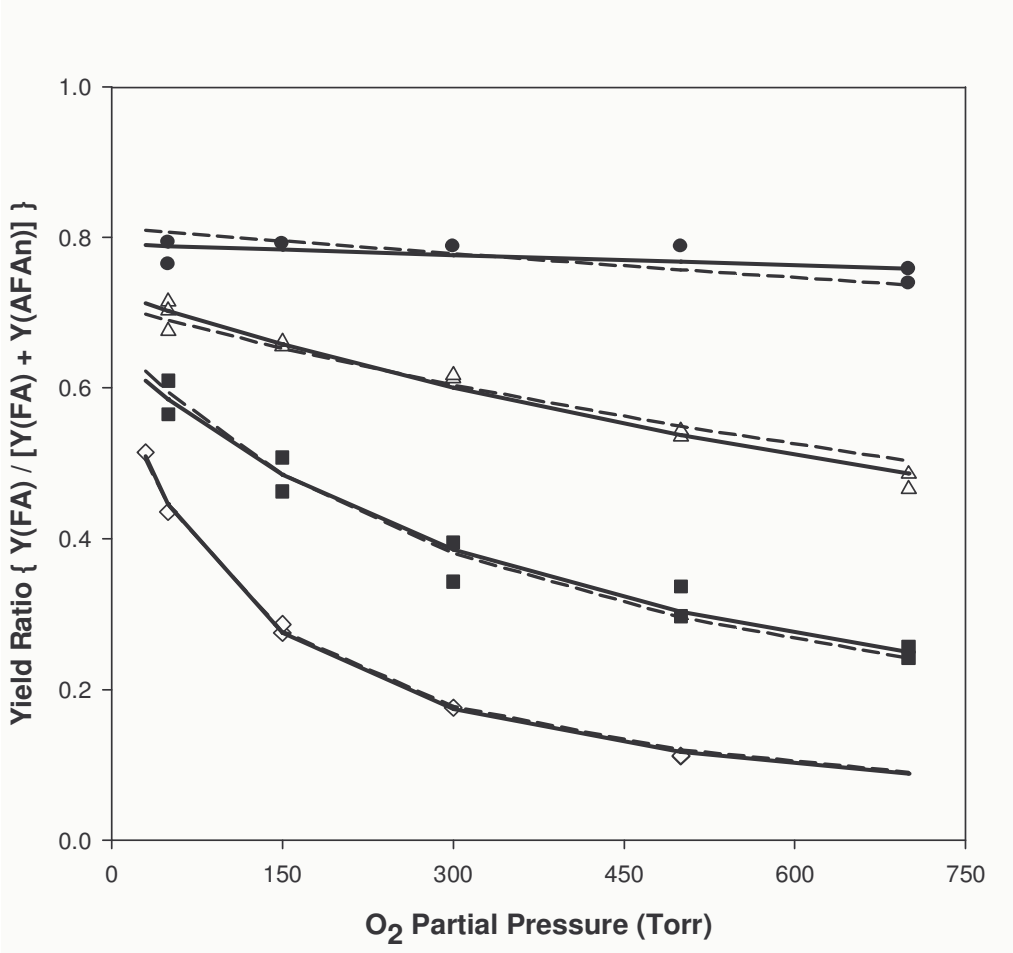

Figure 4: Observed (uncorrected) product concentrations versus consumption of ethyl acetate following photolysis of mixtures of Cl_2 and ethyl acetate in 750 Torr synthetic air at 298 K. Open circles, CO_2; filled circles, acetic acid; open triangles, CO; filled triangles, AAn; squares, formaldehyde. Lines are linear least-squares fits to the CO_2, acetic acid, and AAn data.

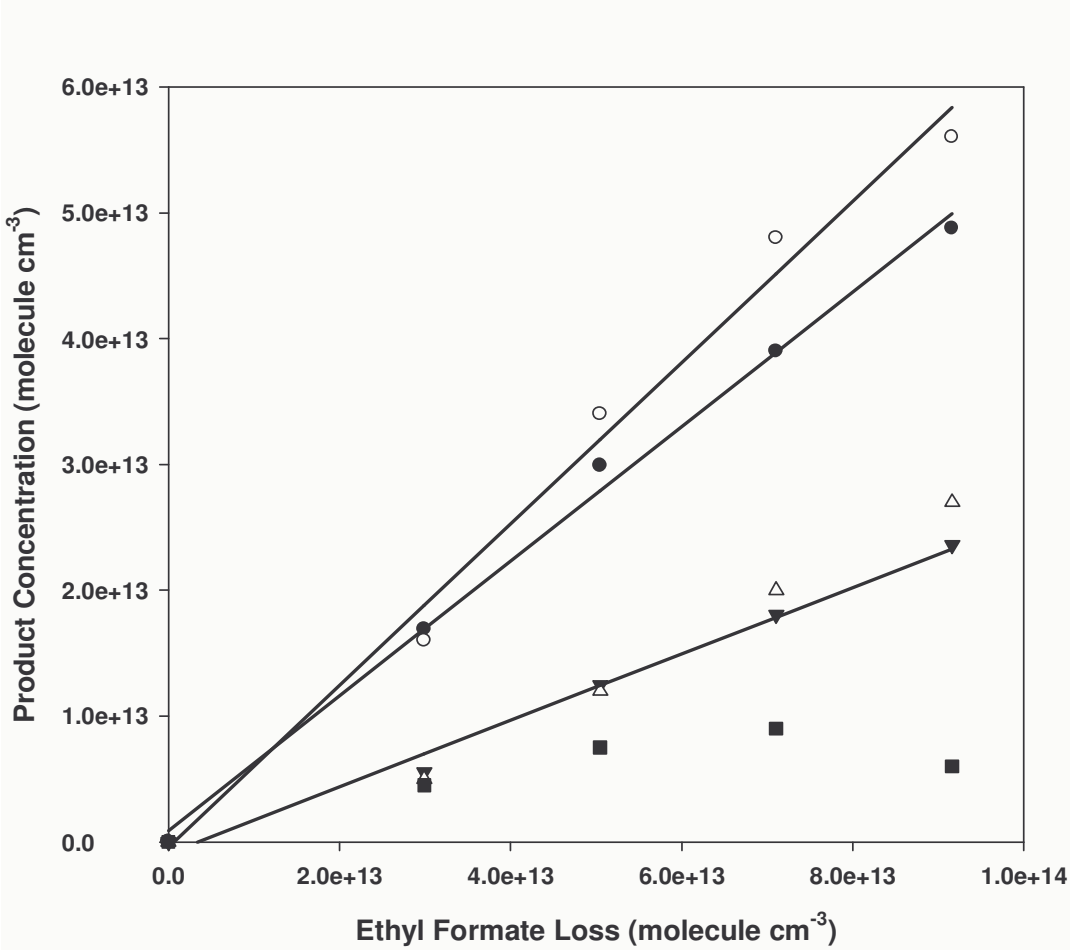

Figure 5: Product yield data { Y(AA) / [Y(AA) + Y(AAn)] } obtained from Cl-atom initiated oxidation of ethyl acetate as a function of O_2 partial pressure. Symbols represent measured data – solid circles 325 K; open circles, 298 K; solid triangles, 273 K; open triangles, 249 K. Solid lines are fits to the data at each individual temperature, dashed lines are results of a fit to the entire dataset, see text for details.

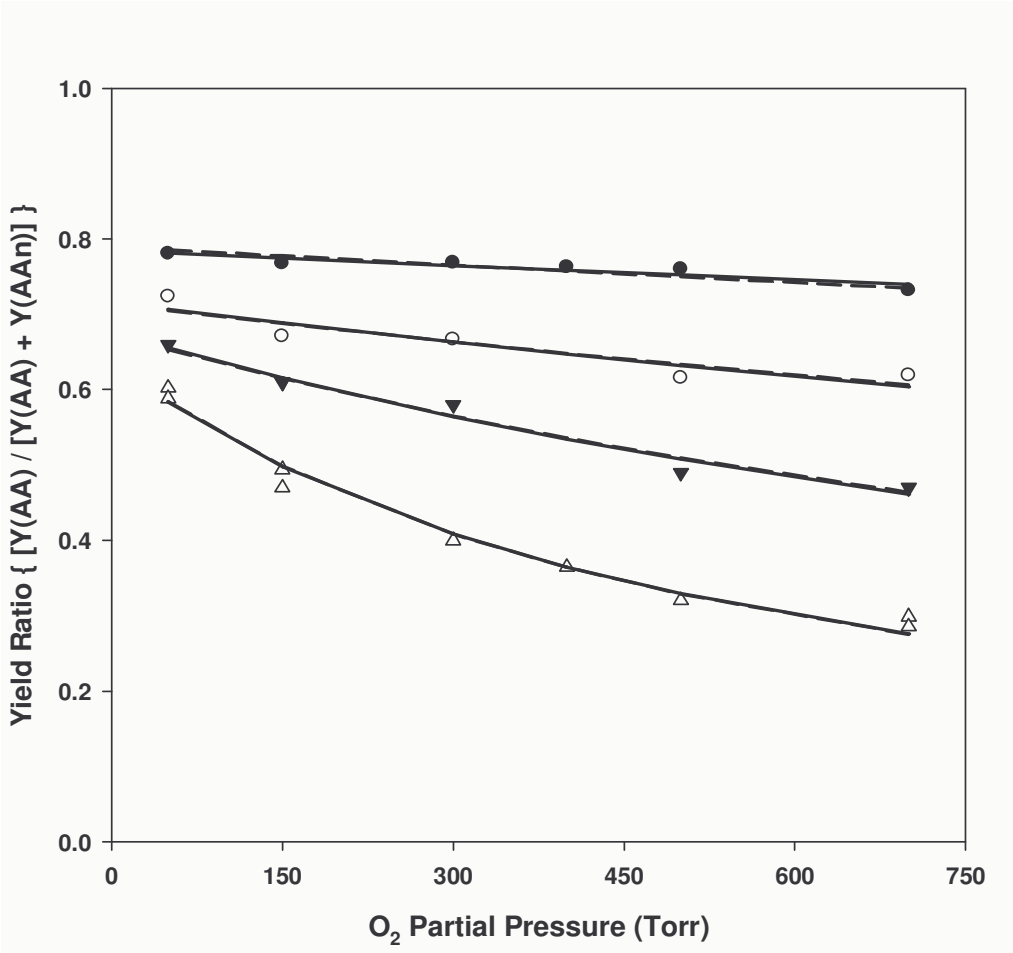

Figure 6: Rate coefficient data for the α-ester rearrangement (relative to its reaction with O_2) for methyl formate (open triangles), methyl acetate (filled triangles), ethyl formate (open circles) and ethyl acetate (filled circles). Solid lines are fits of the simple Arrhenius expression, $k_{\alpha\text{-ester}} / k_{O2} = A \exp(-B/T)$, to the measured data. Dashed lines are obtained by fitting the entire dataset simultaneously, under the assumption that the A-factor is identical for all four systems, see text for details. Methyl formate and methyl acetate data are those reported in [16].